Journal of Alloys and Compounds 854 (2021) 156341

Contents lists available at ScienceDirect

Journal of Alloys and Compounds

journal homepage: http://www.elsevier.com/locate/jalcom

Crystal structure and phase stability of Co_2N: A combined first-principles and experimental study

Yuji Ikeda [a, *], Tanja S. Lehmann [b], Marc Widenmeyer [a, c], Mauro Coduri [d, 1], Blazej Grabowski [a], Rainer Niewa [b, *]

[a] Institute for Materials Science, University of Stuttgart, Pfaffenwaldring 55, 70569 Stuttgart, Germany
[b] Institute of Inorganic Chemistry, University of Stuttgart, Pfaffenwaldring 55, 70569 Stuttgart, Germany
[c] Department of Materials and Earth Sciences, Materials and Resources, Technical University of Darmstadt, Alarich-Weiss-Straße 2, 64287 Darmstadt, Germany
[d] European Synchrotron Radiation Facility, 71 Avenue des Martyrs, 38000 Grenoble, Cedex 9, France

ARTICLE INFO

Article history:
Received 11 June 2020
Received in revised form
25 June 2020
Accepted 7 July 2020
Available online 6 August 2020

Keywords:
Cobalt nitrides
Phase stability
First-principles calculations
X-ray diffraction
Differential scanning calorimetry

ABSTRACT

The crystal structure and phase stability of Co_2N are revisited based on experiments and first-principles calculations. Powder X-ray diffraction (PXRD) measurements and Rietveld refinements clearly confirm that the stable crystal structure of Co_2N is an isotype of η-Fe_2C and Co_2C with the space group *Pnnm* rather than the closely related ζ-Fe_2N with the space group *Pbcn*. The refined lattice parameters of Co_2N in the *Pnnm* structure are a = 4.6108(1) Å, b = 4.3498(1) Å, c = 2.85592(7) Å, obtained from X-ray diffraction using synchrotron radiation. Furthermore, differential scanning calorimetry (DSC) with subsequent diffraction experiments reveal an endothermal transition to an ε-type order at 398 °C followed by an exothermal decomposition at 446 °C. First-principles density-functional-theory (DFT) calculations including the Hubbard U correction (DFT+U) demonstrate that it is essential for transition metal nitrides to consider strong electron correlation to predict the correct experimental structure and magnetic state. In particular, an effective value of U_{eff} = 2.75 eV can be utilized to obtain an antiferromagnetic *Pnnm* phase of Co_2N in agreement with experiments.

© 2020 The Authors. Published by Elsevier B.V. This is an open access article under the CC BY-NC-ND license (http://creativecommons.org/licenses/by-nc-nd/4.0/).

1. Introduction

3*d* transition metal nitrides are an interesting and long-standing topic for science and industry because of their unique properties such as hardness and corrosion resistance [1]. Yet, their synthesis remains challenging. Direct nitriding reactions between a metal and nitrogen at ambient pressure often do not lead to the desired nitride, particularly for highly nitrided phases and for the late transition metal nitrides in general, due to thermodynamic reasons [1,2]. As regards the cobalt nitrides, the first successful synthesis dates back to 1901 [3] when the formation of a cobalt nitride with the composition of Co_4N_2 (= Co_2N) was proposed. Until now four cobalt nitrides have been established, namely CoN (three possible modifications: sphalerite-, rock-salt-, and NiAs-type [2,4–7]), Co_2N [8], Co_3N [8], and Co_4N [9]. Additionally, during laser-heating in nitrogen at high pressures a marcasite-type pernitride with a composition of CoN_2 was obtained [7]. Besides the binary phases, ternary cobalt nitrides such as Co_2Mo_3N [10], Co_3Mo_3N [10], and $Li_{3-2x}Co_xN$ [11] are known.

For the production of Co_2N, which is in our focus, there are several possibilities: Juza and Sachsze [8] reported the ammonolysis of different starting materials, which partially had to be reduced in H_2-flow in an initial step prior to the nitridation in ammonia. The direct reaction between Co and N_2 requires high-pressure high-temperature conditions (supercritical nitrogen fluid at 1527 °C and about 10 GPa using a diamond anvil cell and YAG laser heating) to form Co_2N [2]. Another reported synthetic route uses a supercritical ammonia-methanol mixture between 170 °C and 290 °C at about 16 MPa to achieve nanostructured particles of Co_2N [12]. Direct current reactive sputtering deposition was applied to obtain thin films of Co_2N in a mixture with other cobalt nitrides [13]. Recently, we have obtained rather well crystallized

* Corresponding authors.
E-mail addresses: yuji.ikeda@imw.uni-stuttgart.de (Y. Ikeda), rainer.niewa@iac.uni-stuttgart.de (R. Niewa).
[1] Present address: Department of Chemistry and INSTM, Viale Taramelli 16, 27100 Pavia, Italy.

https://doi.org/10.1016/j.jallcom.2020.156341
0925-8388/© 2020 The Authors. Published by Elsevier B.V. This is an open access article under the CC BY-NC-ND license (http://creativecommons.org/licenses/by-nc-nd/4.0/).

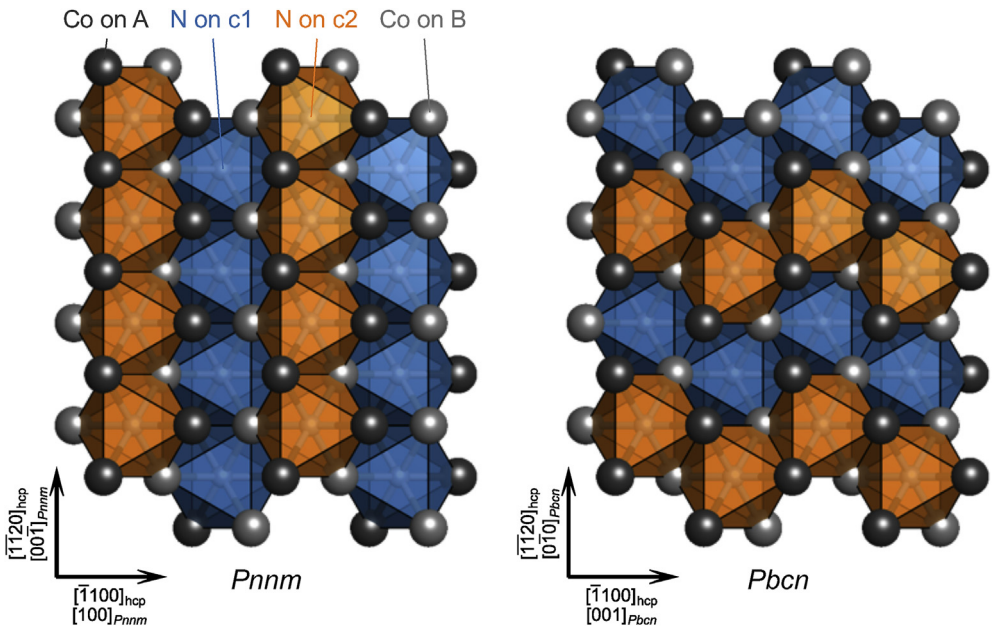

Fig. 1. Schematic representation of Co_2N in the *Pnnm* and *Pbcn* structures from the direction perpendicular to the close-packed Co layers. Dark and light gray spheres represent Co atoms in the A and B layers, respectively. Blue and orange octahedra show the N sites in the c1 and the c2 layers, respectively. Orientation relations between the ideal hcp Co lattice and Co_2N are also shown. Visualization was performed using VESTA [23]. (For interpretation of the references to colour in this figure legend, the reader is referred to the Web version of this article.)

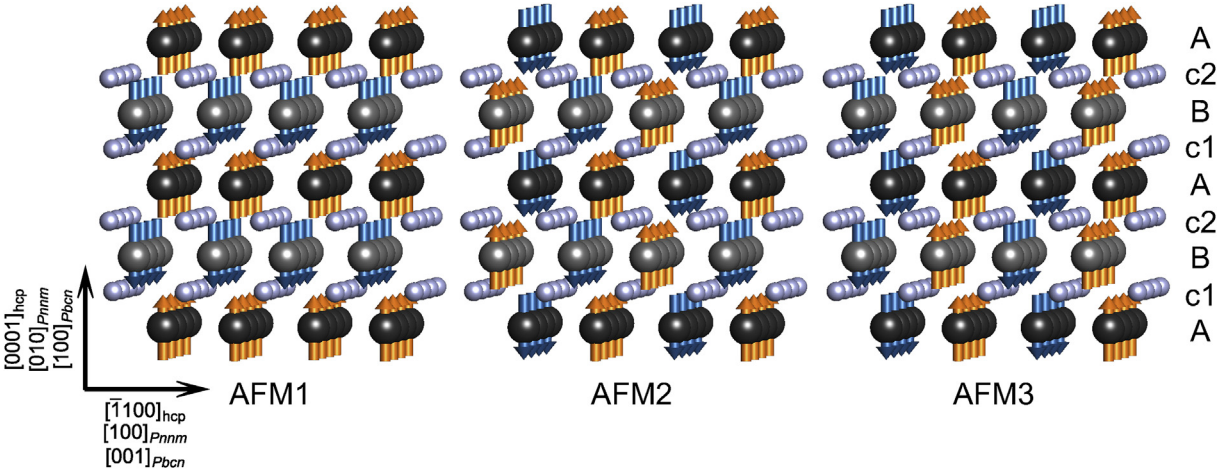

Fig. 2. Schematic representation of the collinear AFM states considered in the present first-principles calculations. Dark and light gray spheres represent the Co atoms in the A and the B layers, respectively. Small white spheres show the N sites in the c1 and the c2 layers, half of which are occupied in a different manner depending on the crystal structure as shown in Fig. 1. Blue and orange arrows on the Co atoms represent the spin-up and the spin-down magnetic moments, respectively. Orientation relations between the ideal hcp Co lattice and Co_2N (both in the *Pnnm* and the *Pbcn* structures) are also shown. (For interpretation of the references to colour in this figure legend, the reader is referred to the Web version of this article.)

Co_2N samples of good purity from decomposition of the azide precursor $[Co(NH_3)_5N_3]Cl_2$ in flowing ammonia [14].

The crystal structure of Co_2N was already reported to be isotypic to the structure of the respective cobalt carbide (Co_2C) and iron carbide (η-Fe_2C) with the corresponding compositions [15,16], i.e., to the $CaCl_2$-type structure with the space group *Pnnm*. Information on structural data of Co_2N is, however, rather limited [2,15], contingent on its challenging synthesis. For example, during the formation of Co_2N, hexagonal Co_3N is a frequent by-product, difficult to avoid and also difficult to detect due to strongly overlapping reflections in the diffraction patterns [8,14]. A further challenging aspect is the structural similarity of the *Pnnm* structure to the α-PbO_2-type structure with space group *Pbcn* that is found for the chemically closely related iron nitride phase ζ-Fe_2N [17]. One can consider *Pbcn* Co_2N by replacing Fe in ζ-Fe_2N with Co and modification of lattice parameters. The thus obtained *Pbcn* Co_2N is topologically similar to the *Pnnm* Co_2N as emphasized in Fig. 1. In both structures, the Co atoms form the motif of a hexagonal close-packing (hcp) distorted into an orthorhombic structure. Within this hcp of Co, N atoms occupy half of the octahedral voids. Consequently, the resulting arrangement has the layer sequence of "⋯-A-c1-B-c2-A-c1-B-c2-⋯", where c1 and c2 indicate the interstitial N layers sandwiched by the hcp Co layers of A and B. In both the *Pnnm* and the *Pbcn* structures all the Co_6N octahedra share their

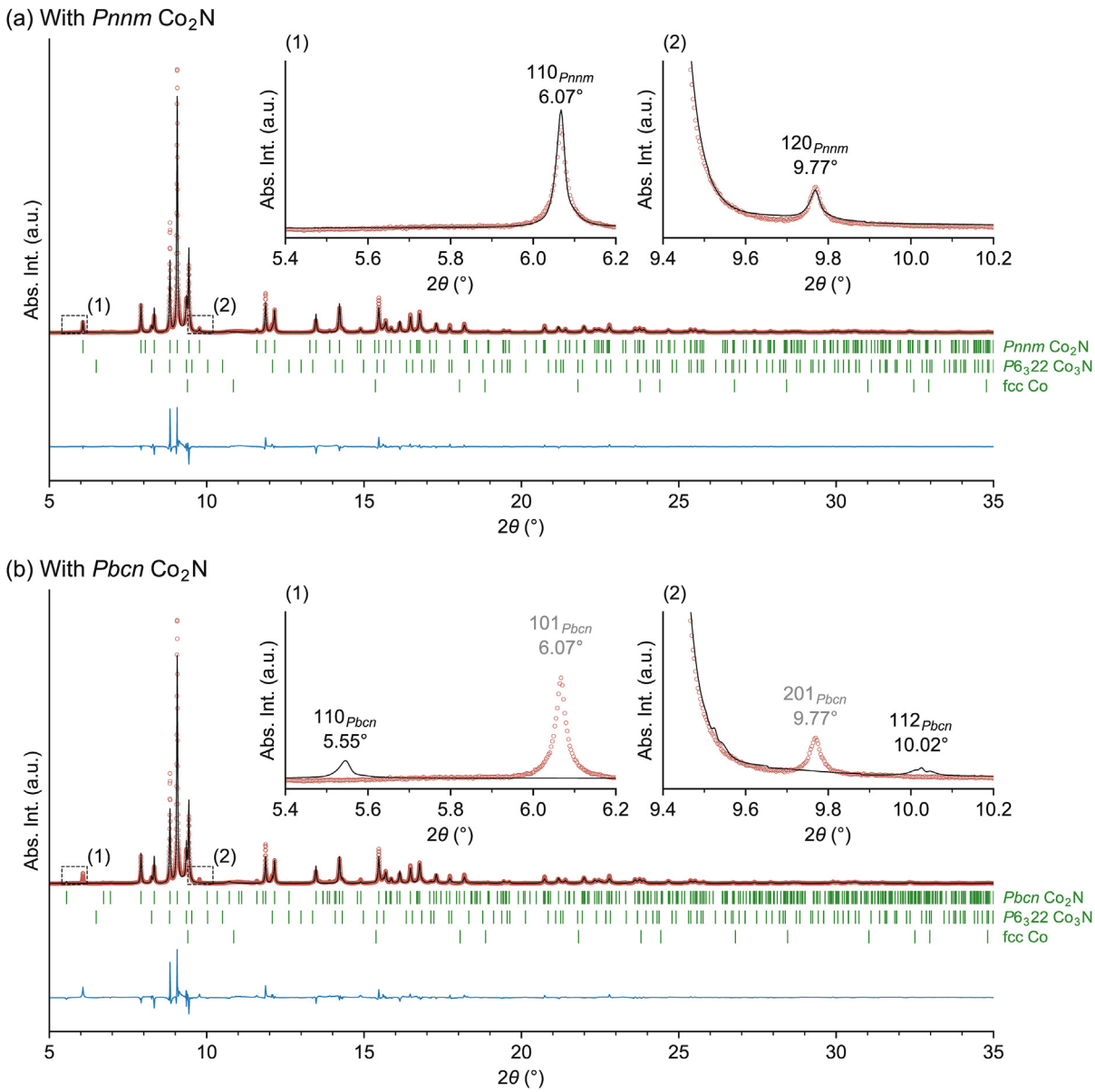

Fig. 3. Graphical representation of the Rietveld refinements of the crystal structure of Co_2N in (a) *Pnnm* and in (b) *Pbcn* (ζ-Fe_2N-type crystal structure) against PXRD obtained with synchrotron radiation (λ = 0.335914(5) Å). The measured (red dots), calculated (black line), and the difference (observed−calculated, blue line) patterns as well as the Bragg positions of Co_2N (green vertical bars, top row), Co_3N (middle) and fcc Co (bottom) are shown. The insets enlarge the regions with 2θ ranges of (1) 5.4–6.2° and (2) 9.4–10.2°, surrounded by small dashed rectangles, where forbidden reflections of the *Pbcn* structure are indicated by gray text. (For interpretation of the references to colour in this figure legend, the reader is referred to the Web version of this article.)

edges and corners. The *only* difference between the two structures is the N ordering. Namely, in the *Pnnm* structure N atoms are arranged in straight corridors in each of the c1 and the c2 layers, while in the *Pbcn* structure N atoms feature a zigzag arrangement. A conclusive structure identification needs to take this structural similarity between *Pnnm* and *Pbcn* carefully into account, and this is one goal of the present study.

First-principles calculations are nowadays very common for transition metal oxides, carbides, as well as nitrides. For transition metal oxides, the importance of strong electron correlation is well accepted, and it is essential to consider the proper methodology, such as density-functional-theory (DFT) including the Hubbard *U* correction, i.e., DFT+*U* [18]. For transition metal carbides and nitrides, in contrast, research on the impact of strong electron correlation is rather limited, although its importance has been reported [19–21]. A good example is given by CrN for which pure DFT wrongly predicts a nonmagnetic (NM) phase to be the most stable [21]. Only when considering the strong electron correlation, the experimentally observed antiferromagnetically (AFM) ordered orthorhombic phase [22] can be correctly stabilized [21]. For Co_2N, detailed investigations on the impact of strong electron correlation have not been reported yet, and this is the second goal of the present study.

Thus, in this paper, the phase stability and the structural parameters of Co_2N are revisited based on both experiments and first-principles calculations. Improved structural parameters are derived by performing powder X-ray diffraction (PXRD) measurements with synchrotron radiation. Rietveld refinements allow us to substantiate that the crystal structure of Co_2N has *Pnnm* symmetry. Decomposition of Co_2N at elevated temperatures is also studied using

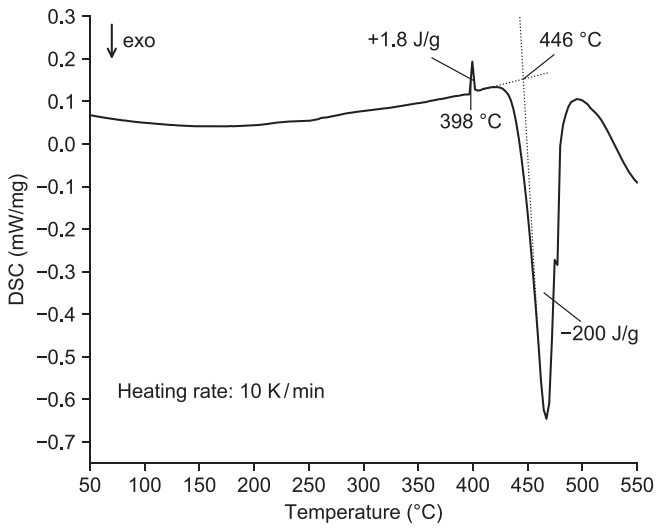

Fig. 4. DSC measurement of Co_2N. The onset temperatures of the peaks and the corresponding enthalpy changes are also shown.

Table 1
Detailed data of Rietveld refinements for the synchrotron-radiation PXRD (Fig. 3(a)) obtained in the present study. Source: synchrotron (ID22, ESRF, Grenoble, France). Temperature: 295 K. Pressure: 101.325 kPa. Wavelength: 0.335914(5) Å. *d*-space range: 0.501–4.77 Å. $R_p = 9.94\%$. $R_{wp} = 13.5\%$. $\chi^2 = 7.51$. The residual values of the Rietveld refinements are defined as $R_p\ (\%) = 100 \sum_i |Y_{obs,i} - Y_{calc,i}| / \sum_i |Y_{obs,i}|$ and $R_{wp}\ (\%) = 100 \left(\sum_i w_i |Y_{obs,i} - Y_{calc,i}|^2 / \sum_i w_i |Y_{obs,i}|^2\right)^{1/2}$, where Y_{obs} and Y_{calc} are measured and calculated intensities, respectively.

	Co_2N	Co_3N	Co
Crystal system	orthorhombic	hexagonal	cubic
Space group (No.)	*Pnnm* (58)	$P6_322$ (182)	$Fm\bar{3}m$ (225)
Z	2	2	4
Chemical formula	Co_2N	$Co_3N_{1.14}$	Co
Formula weight (Da)	131.87	192.77	58.93
a (Å)	4.6108(1)	4.6578(4)	3.55452(7)
b (Å)	4.3498(1)		
c (Å)	2.85592(7)	4.3553(5)	
α (°)	90	90	90
β (°)	90	90	90
γ (°)	90	120	90
V (Å^3)	57.278(3)	81.333(4)	44.56(3)

differential scanning calorimetry (DSC). A detailed DFT+*U* analysis is performed to elucidate the impact of on-site electron correlation for various magnetic phases as a function of the effective *U* parameter. We establish a parameter range for *U* which leads to the experimentally observed AFM *Pnnm* phase as the ground state.

2. Experimental details

2.1. Synthesis

All manipulations for the synthesis of Co_2N were carried out in an argon filled glovebox (MBraun, $p(O_2) < 0.1$ ppm). Metastable Co_2N was synthesized by ammonolysis of $[Co(NH_3)_5N_3]Cl_2$. A modified reaction protocol based on the one reported in literature [14] was used: (i) 350 °C (8 h) or (ii) 450 °C (12 h) followed by cooling to 350 °C within 12 h. In all cases an ammonia flow (> 99.999 %) of 60 ml/min was applied. The precursor $[Co(NH_3)_5N_3]Cl_2$ was synthesized according to Linhard and Flygare [24]; $CoCl_2 \cdot 6H_2O$ was dissolved in a small amount of deionized water and mixed with an aqueous solution of NaN_3, NH_4Cl, and NH_3. This mixture was stirred at 60 °C for 2 h. After that the reaction mixture was cooled down in an ice bath for a complete precipitation. The obtained precipitate was washed with diluted hydrochloric acid and ethanol several times. To further purify the precursor by recrystallization, it was dissolved in deionized water and precipitated by a careful addition of concentrated hydrochloric acid. After washing with ethanol the product was dried at 50 °C for several days.

2.2. Characterization

PXRD measurements were carried out at ambient temperature in the following two conditions:

- At the ID22 beamline of the European Synchrotron Radiation Facility (ESRF) in Grenoble, France (λ = 0.335914(5) Å) using a 9-element detector array (high resolution setup). The data collection was performed in a 2θ range of 5–35° in transmission geometry. The sample of Co_2N was located in a 0.7 mm diameter Kapton® capillary and installed parallel to the axis of the diffractometer. This was performed for Rietveld refinements of the structure of Co_2N.
- On a STOE Stadi-P diffractometer equipped with a Ge(111) monochromator and a Mythen 1K detector using Mo-$K_{\alpha 1}$ radiation. The data collection was performed in a 2θ range of 5–65° in transmission geometry. This measurement was performed in order to check the sample quality prior to the measurements at the synchrotron source and to investigate the existing phases after the DSC experiments.

Rietveld refinements of Co_2N were carried out using the FullProf program suite [25].

DSC experiments were performed on a DSC204F1 Phoenix (Netzsch Gerätebau GmbH) in cold-welded aluminium pans using a heating rate of 10 K/min in flowing argon atmosphere.

Table 2
Comparison of structural parameters of Co_2N, Co_3N, and fcc Co obtained from Rietveld refinements for the present synchrotron-radiation PXRD data with those from previous experimental studies. In *Pnnm* Co_2N, Co and N atoms are located at the Wyckoff sites of 4*g* (*x*, *y*, 0) and 2*a* (0, 0, 0), respectively. In hexagonal $P6_322$ Co_3N, Co atoms are located at 6*g* (*x*,0, 0), while N atoms are located both at 2*c* (1 /3, 2 /3, 1 /4) and at 2*b* (0, 0, 1 /4). In fcc $Fm\bar{3}m$ Co, Co atoms are located at the Wyckoff site of 4*a* (0, 0, 0). The values obtained from the present DFT+*U* calculations for the AFM3 Co_2N with $U_{eff} = 2.75$ eV are also displayed.

	Reference	*a* (Å)	*b* (Å)	*c* (Å)	*x* (Co)	*y* (Co)
Co_2N	Present	4.6108(1)	4.3498(1)	2.85592(7)	0.3242(1)	0.2643(1)
	Clarke and Jack [15]	4.6056(10)	4.3443(10)	2.8535(5)	0.33	0.26
	Hasegawa and Yagi [2]	4.662(9)	4.332(5)	2.749(9)	N/A	N/A
	DFT+*U*	4.828	4.490	2.828	0.30	0.26
Co_3N	Present	4.6578(4)		4.3553(5)	0.332(3)	
	Widenmeyer et al. [14]	4.6435(2)		4.3534(2)	0.336(1)	
Co	Present	3.5452(7)				
	Owen and Jones [38]	3.5441				

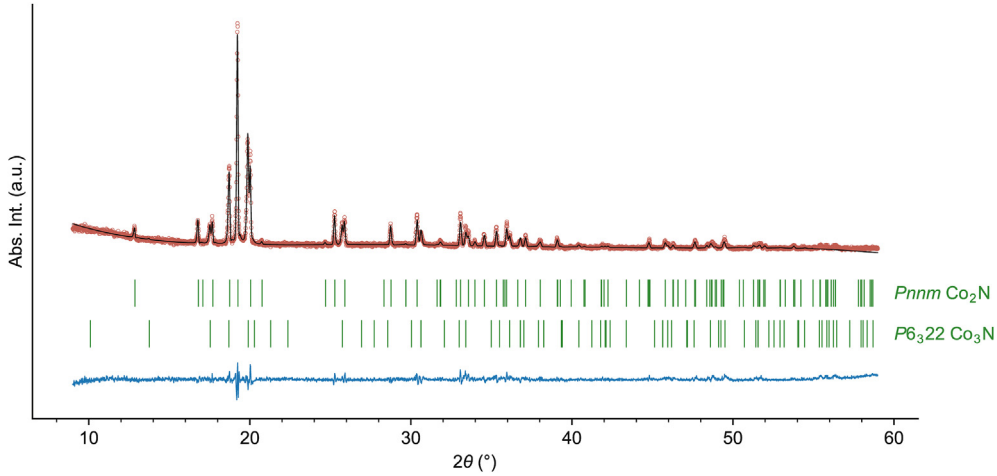

Fig. 5. Graphical representation of the Rietveld refinements of Co_2N against PXRD with Mo-$K_{\alpha1}$ radiation ($\lambda = 0.7093$ Å) after the DSC measurement in Fig. 4. The measured (red dots), calculated (black line), and the difference (observed−calculated, blue line) patterns as well as the Bragg positions of Co_2N (green vertical bars, top row) and Co_3N (bottom) are shown. (For interpretation of the references to colour in this figure legend, the reader is referred to the Web version of this article.)

Table 3
Detailed data of Rietveld refinements after the DSC measurement in Fig. 4. Source: STOE Stadi P, Mo-$K_{\alpha1}$. Temperature: 295 K. Pressure: 101.325 kPa. Wavelength: 0.7093 Å. *d*-space range: 0.77–4.08 Å. $R_p = 9.49\%$. $R_{wp} = 12.3\%$. $\chi^2 = 1.18$. The definitions of the residual values of Rietveld refinements are given in Table 1.

	Co_2N	Co_3N
Crystal system	orthorhombic	hexagonal
Space group (No.)	*Pnnm* (58)	$P6_322$ (182)
Z	2	2
Chemical formula	Co_2N	$Co_3N_{1.34}$
Formula weight (Da)	131.87	195.57
a (Å)	4.6107(3)	4.6518(3)
b (Å)	4.3538(3)	
c (Å)	2.8555(2)	4.3664(4)
α (°)	90	90
β (°)	90	90
γ (°)	90	120
V (Å^3)	57.322(7)	81.83(1)

3. Computational details

For the DFT calculations, we modeled Co_2N in *Pnnm* and *Pbcn* symmetry using unit cells with 6 and 12 atoms, respectively. In the *Pnnm* structure, Co and N occupy the 4*g* and the 2*a* Wyckoff positions, respectively. In the *Pbcn* structure, Co and N occupy the 8*d* and the 4*c* Wyckoff positions, respectively. We employed the projector augmented wave method [26] and the generalized gradient approximation (GGA) of the Perdew-Burke-Ernzerhof (PBE) form [27] implemented in the VASP code [28,29] in combination with the provided potentials [30]. The 3*d*4*s* and the 2*s*2*p* orbitals of Co and N, respectively, were treated as valence states. The plane-wave cutoff was set to 550 eV. Γ-centered 12×12×20 and 12×10×12 *k*-point meshes were applied for the *Pnnm* and the *Pbcn* structures, respectively, and the Methfessel-Paxton scheme [31] was employed with a smearing width of 0.1 eV. Total energies were minimized until they were converged to within 10^{-5} eV per unit cell. Cell volume, cell shape, and internal atomic positions were optimized so that the forces on atoms and the stress components on the unit cells are less than 2×10^{-4} eV/Å and 2×10^{-3} eV/Å^3, respectively. Strong on-site electron correlation was considered employing the rotationally invariant DFT+*U* formalism of Dudarev et al. [32], with $U_{eff} \equiv U - J$ varied in a range of 0–4 eV. Volumes, charges, and magnetic moments on Co and N atoms were computed based on the Bader analysis [33] employing the Yu-Trinkle algorithm [34] as implemented by Henkelman et al. [35–37].

In a previous experimental study [14], Co_2N was found to be in an AFM state at very low temperatures with a Néel temperature of 10 K. To investigate the impact of magnetic ordering on the phase stability of Co_2N, in the present first-principles calculations, we conducted collinear spin-polarized calculations of several model AFM states (Fig. 2) as well as of the ferromagnetic (FM) and the NM states.

The formation energy per atom, ΔE_f, of Co_2N was computed as

$$\Delta E_f = \frac{1}{3}\left\{E(Co_2N) - \left[2E(Co) + \frac{1}{2}E(N_2)\right]\right\}, \quad (1)$$

where $E(Co_2N)$ is the energy of Co_2N per formula unit. The energy of pure FM hcp Co, $E(Co)$, was computed by optimizing the cell volume and the cell shape for the *same* U_{eff} as that used for Co_2N. A 22×22×14 *k*-point mesh was used to sample the Brillouin zone of the two-atom Co hcp cell. The energy of a nitrogen molecule, $E(N_2)$, was computed with spin-polarization and by optimizing the bond distance. To minimize the interaction with periodic images, a large unit cell of 20 Å × 20 Å × 20 Å and the Γ-point for sampling the Brillouin zone were used.

4. Results and discussion

4.1. Rietveld refinements

Due to its metastable nature, the synthesis of bulk Co_2N in high purity remains rather difficult. Further optimization of the ammonolysis route of the $[Co(NH_3)_5N_3]Cl_2$ precursor [14,24] by variation of decomposition and annealing temperature, cooling rate, and flow conditions of ammonia finally reproducibly led to samples, which contained only small admixtures of Co_3N (strictly, Co_3N_{1+x} with $x = 0.14(5)$) and face-centered cubic (fcc) Co. Due to severe reflection overlap, these impurity phases are only noticeable on close inspection of the PXRD patterns and reveal as shoulders of reflections belonging to the title phase or by small intensity deviations from expected values. The graphical representation of the Rietveld refinements of the synchrotron-radiation PXRD data is presented in Fig. 3(a), and further details of the Rietveld refinements are summarized in Table 1. The dominant phase is represented by Co_2N with 83(1) wt.%, followed by the impurity phases of Co_3N (12(1) wt.%) and

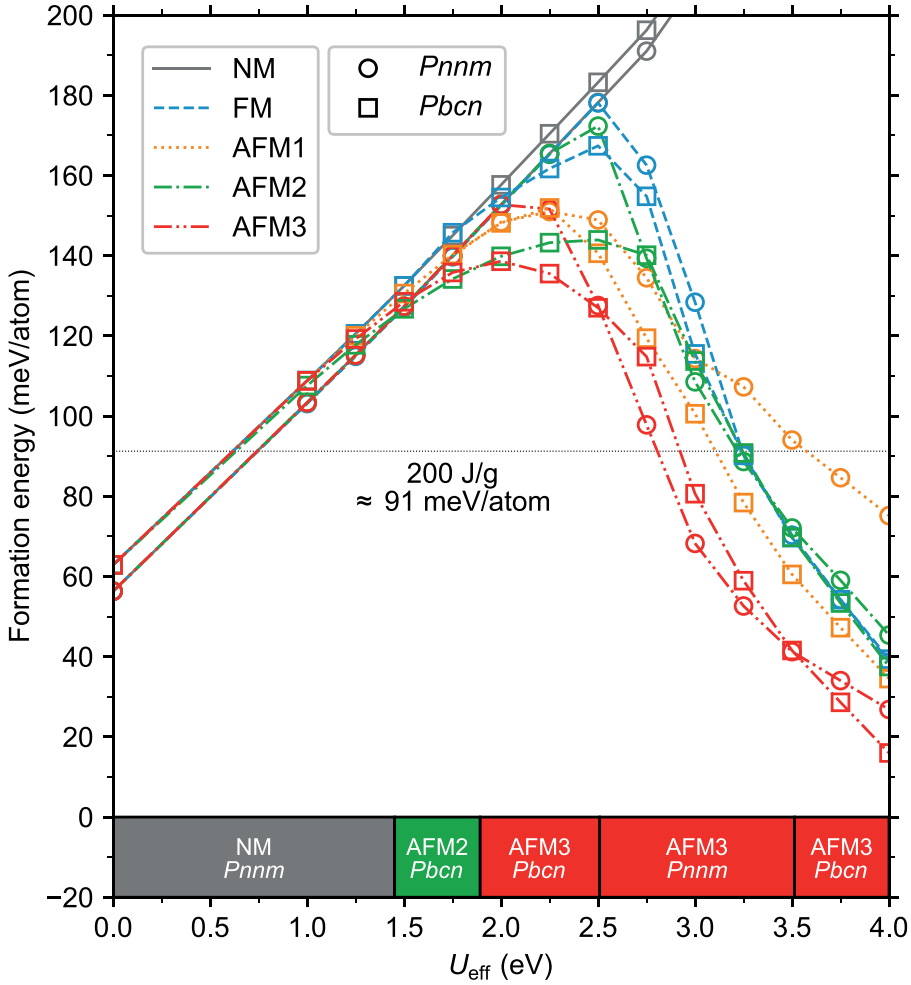

Fig. 6. Formation energies per atom ΔE_f of Co_2N as a function of U_{eff} from the present DFT+U calculations. The obtained ground state at each U_{eff} is shown at the bottom. The experimental formation energy of Co_2N expected from the present DSC measurement is shown by the thin dotted horizontal black line.

fcc Co (5(1) wt.%). In Table 2 the observed lattice parameters of both nitride phases and fcc Co are compared with earlier reported data and confirm good agreement. Deviations may be due to slight variations in nitrogen content of the different phases studied, as such interstitial transition metal nitrides are generally prone to show homogeneity ranges [1]. A composition of $Co_3N_{1.14(5)}$ was determined for the nitride impurity phase, which is in reasonable agreement with the previously reported value of $Co_3N_{1.1}$ determined by thermogravimetric analysis [14]. Fcc Co represents the high temperature phase of cobalt stable above about 420 °C [39] but may be readily quenched to room temperature [38]. For comparison, Rietveld refinements of the crystal structure of Co_2N in *Pbcn*, i.e., in the ζ-Fe_2N-type structure, are presented in Fig. 3(b). While at a first glance a similar Rietveld pattern to that for the *Pnnm* structure is obtained (because of the similarity of the *Pnnm* and the *Pbcn* structures as described in Fig. 1), a closer inspection reveals that e.g. the reflections measured at $2\theta = 6.07°$ and $2\theta = 9.77°$ are not reproduced. These reflections formally correspond to 101_{Pbcn} and 201_{Pbcn}, respectively, but are forbidden for *Pbcn* according to the reflection condition of $l = 2n$ for $h0l$ related to *c*-gliding [40]. The refinements with the *Pbcn* structure, furthermore, misproduce the 110_{Pbcn} and the 112_{Pbcn} reflections at $2\theta = 5.55°$ and $2\theta = 10.02°$, respectively, which are not observed in the measured PXRD data. It is thus clearly demonstrated that Co_2N crystallizes in the *Pnnm* structure rather than in the *Pbcn* structure.

4.2. Differential scanning calorimetry (DSC)

Fig. 4 shows the DSC measurement of Co_2N between 20 °C and 550 °C with a heating rate of 10 K/min in an argon atmosphere. At an onset temperature of 398 °C there is a small endothermal signal with an enthalpy of +1.8 J/g followed by a stronger exothermal signal with an enthalpy of −200 J/g at an onset temperature of 466 °C. A sample heated to a slightly higher temperature than the occurrence of the endothermal signal contained two phases, namely Co_2N (67(1) wt.%) and $Co_3N_{1.34}$ (33(1) wt.%), according to PXRD using Mo-$K_{\alpha 1}$ radiation (Fig. 5 and Table 3). This indicates a significant increase of the fraction of the Co_3N phase. Rietveld refinements after the DSC measurement showed a slightly higher nitrogen content in Co_3N_{1+x} ($x = 0.34(15)$) than that before the DSC measurement ($x = 0.14(5)$) via occupation of a further nominally empty octahedral void, as was earlier observed, although to a much smaller extent [14]. A similar increase in nitrogen content is found also in Mn−N [41] and Fe−N [42,43] systems during decomposition of the respective nitride phase. The resulting composition corresponds closely to a Co_2N phase ($Co_3N_{1.34} = Co_2N_{0.90}$) with the

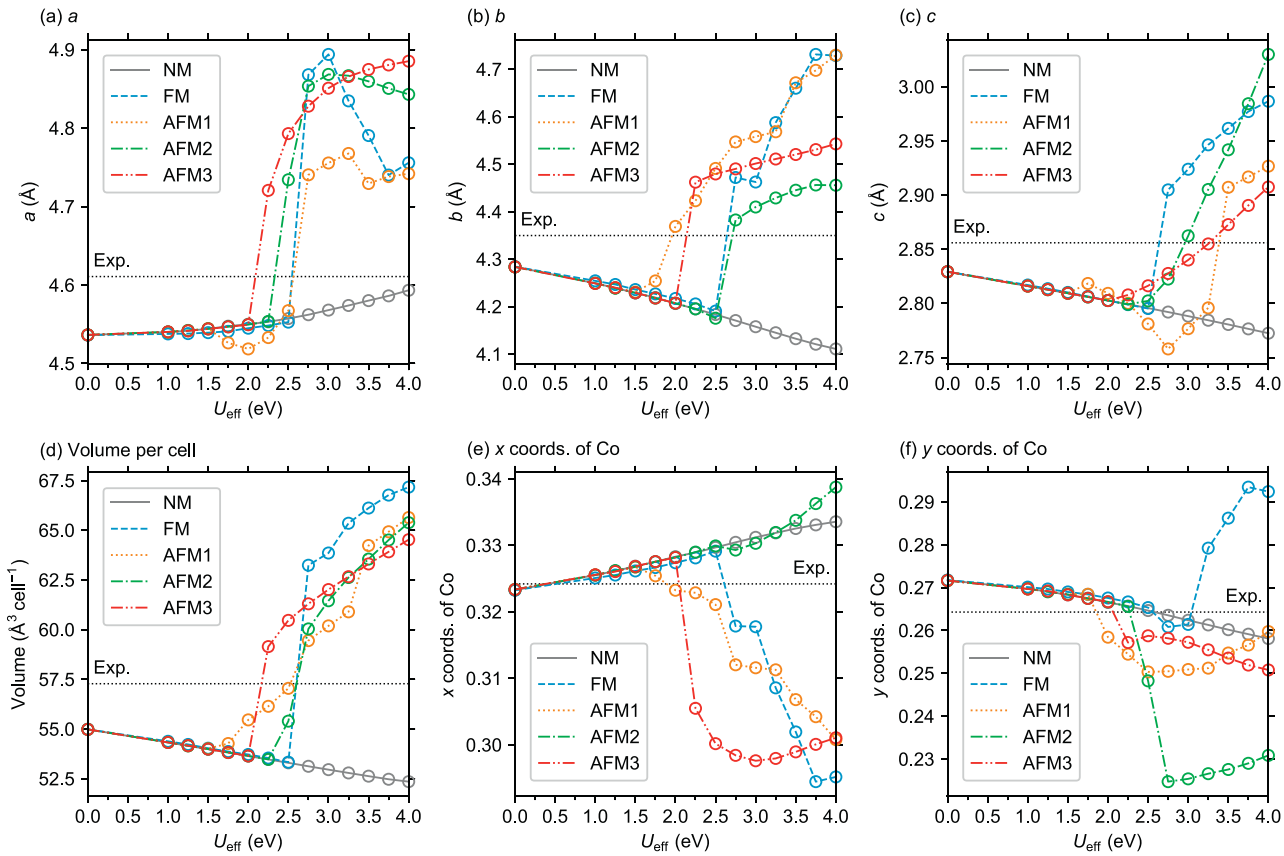

Fig. 7. Structural parameters of *Pnnm* Co_2N obtained from the DFT+*U* calculations. Dotted horizontal black lines show the experimental values obtained in the present study (Table 2).

ε-type order, as similarly known for ε-Fe_3N_{1+x} with *x* up to about 0.5, i.e. ε-Fe_2N [44,45]. Earlier simultaneous differential thermal analysis and thermal gravimetric analysis (DTA/TG) measurements indicated a weight loss starting at around 370 °C with an exothermal signal at 429.6 °C for Co_2N, while Co_3N started to decompose at around 420 °C with an exothermal signal at 593 °C [14]. The exothermal decomposition in every case directly results in the formation of fcc Co.

4.3. First-principles calculations

Fig. 6 shows the formation energies of Co_2N obtained from the DFT+*U* calculations. For the whole investigated range of the effective Hubbard *U* value, i.e., $U_{eff} = 0–4$ eV, all considered phases show positive formation energies ΔE_f, in consistency with the metastability of Co_2N observed in experiments. However, for $U_{eff} = 0$ eV (i.e., pure DFT), all magnetic states converge to the NM state for both the *Pnnm* and the *Pbcn* structures, which is inconsistent with the experimental finding of an AFM state [14]. The magnetic states are rapidly stabilized with respect to the NM state with increasing U_{eff}. In particular, the AFM configurations are preferentially stabilized for $U_{eff} \geq 1.5$ eV. This finding highlights the necessity to consider the strong on-site electron correlation to stabilize the AFM states in agreement with experiment. Yet, although the magnetic state is correctly predicted when utilizing a U_{eff} within 1.5–2.5 eV, the *Pbcn* phase is energetically more stable than *Pnnm*, which is again inconsistent with our detailed experimental analysis provided above. In order to obtain not only the correct magnetic state but also the correct crystallographic structure, i.e., *Pnnm*, as the energetically most stable one, the value of U_{eff} needs to be taken within the range of 2.5–3.5 eV. For a higher U_{eff} (up to the maximum investigated U_{eff} of 4 eV), again the experimentally excluded *Pbcn* phase is energetically more stable than the *Pnnm* phase.

Our calculations highlight that we can obtain simulation results that are consistent with the experimental phase stability and magnetic state only within a limited U_{eff} range of 2.5–3.5 eV. In particular, it is the AFM3 *Pnnm* Co_2N phase that is the most stable for these U_{eff} values. In fact for $U_{eff} = 2.75$ eV, we can also obtain a very good agreement between the *ab initio* formation energy, ΔE_f, and the exothermal phase transition observed from the present DSC measurements, 200 J/g ≈ 91 meV/atom. It is worth mentioning that the U_{eff} range of 2.5–3.5 eV includes the value reported to be suitable for cobalt oxides [18]; i.e., U_{eff} of 3.3 eV which was used to reproduce the experimental oxidation energies from CoO to Co_3O_4 [18]. This U_{eff} value also reproduces the experimentally observed rock-salt-type structure of $CoO_{0.75}N_{0.25}$ at the experimental volume [14]. Our present results further support that a U_{eff} in the 2.5–3.5 eV range should be a safe choice for cobalt nitrides as well as oxides.

For $U_{eff} > 2$ eV, the AFM3 state is energetically more stable than any other considered magnetic state for both the *Pnnm* and the *Pbcn* structures. It should be emphasized that, without the AFM3 state, we would not obtain the *Pnnm* structure to be more stable than the *Pbcn* structure despite the inclusion of the strong on-site electron correlation via DFT+*U*. This reveals the importance of a careful consideration of various magnetic candidate states when investigating cobalt nitrides. Note that the true AFM ground state of

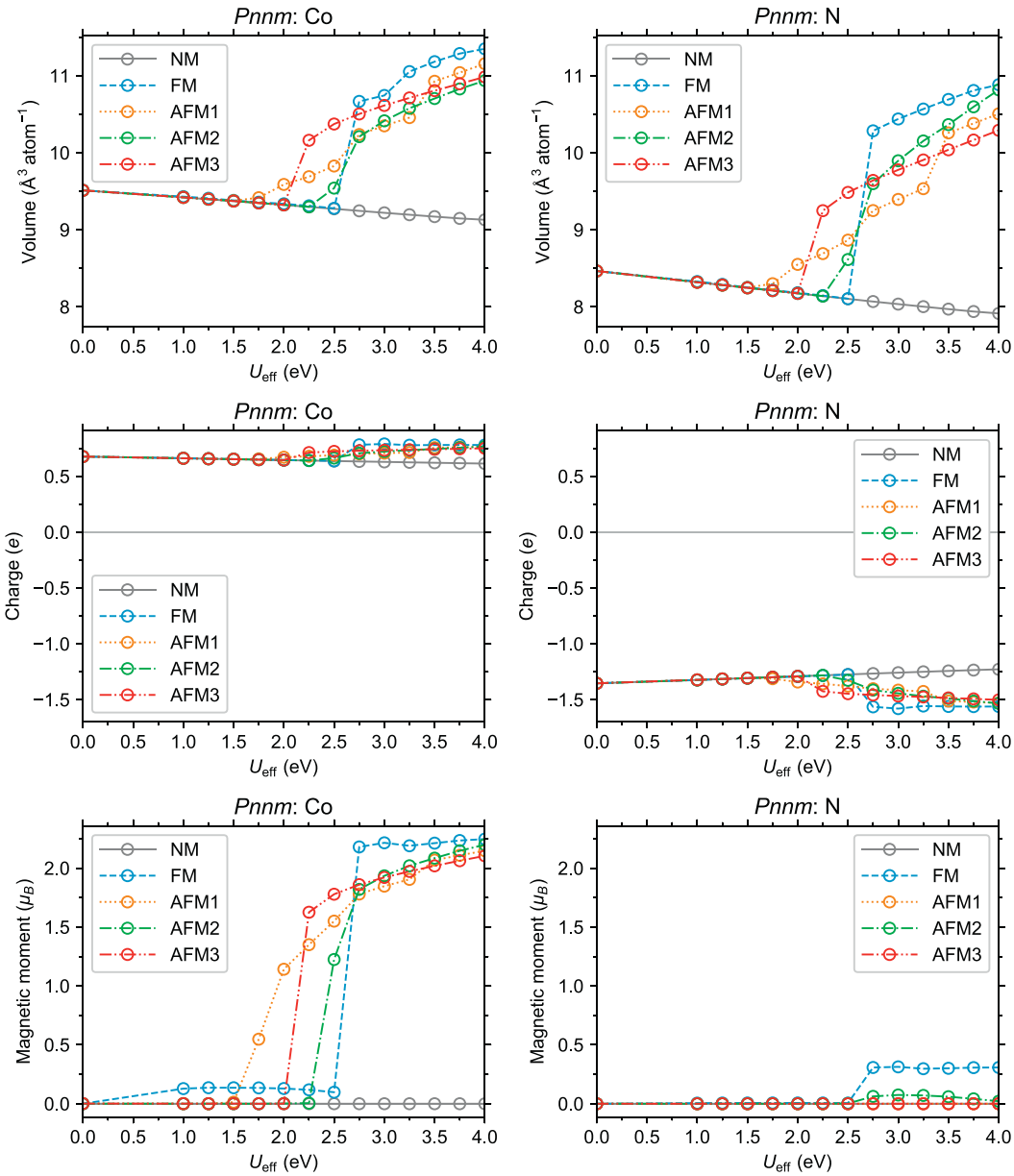

Fig. 8. Local volumes, charges, and magnetic moments on the atoms (top, middle, and bottom columns, respectively) of *Pnnm* Co_2N in the DFT+*U* calculations based on the Bader analysis.

Co_2N might have noncollinear magnetic moments, the consideration of which is beyond the scope of the present study. Nevertheless, the here considered collinear AFM3 state explains well the experimental phase stability and hence can be used to model Co_2N in a rather straightforward manner. Our results thus provide guidance to future first-principles calculations.

Fig. 7 shows the structural parameters of *Pnnm* Co_2N obtained from the DFT+*U* calculations. For the unit cell parameters (Fig. 7(a)–7(c)), the values of the (unrealistic) NM state and of the magnetic states tend to underestimate and overestimate the experimental values, respectively. For the atomic coordinates (Fig. 7(d) and (e)), the situation is less transparent and depends strongly on the magnetic state. Note that there is no single U_{eff} value for which we would observe good agreement for *all* structural parameters, neither for the "good" range of $U_{eff} = 2.5–3.5$ eV nor for the remaining investigated range up to $U_{eff} = 4$ eV. We attribute this to the well-known systematic deviation of DFT lattice parameters [46], which is very likely inherited by the present DFT+*U* calculations. It is, nevertheless, demonstrated that both the magnetic condition and the strong on-site electron correlation largely affect the structural parameters. For example, for $U_{eff} = 2.75$ eV which lies in the range for which we observe the correct structural and magnetic ground state, we find structural parameters as given in Table 2.

Fig. 8 shows the local atomic volumes, charges, and magnetic moments of Co_2N from the DFT+*U* calculations based on the Bader analysis [33]. Co shows a larger atomic volume than N. Magnetic states show larger volumes than the NM state both for Co and for N. It is also found that Co and N are charged positively and negatively, respectively, consistently with their electronegativities (in the definitions of Pauling [47] and Allen [48–50]). Further, the charges are not strongly dependent on the magnetic state. At $U_{eff} = 2.75$ eV,

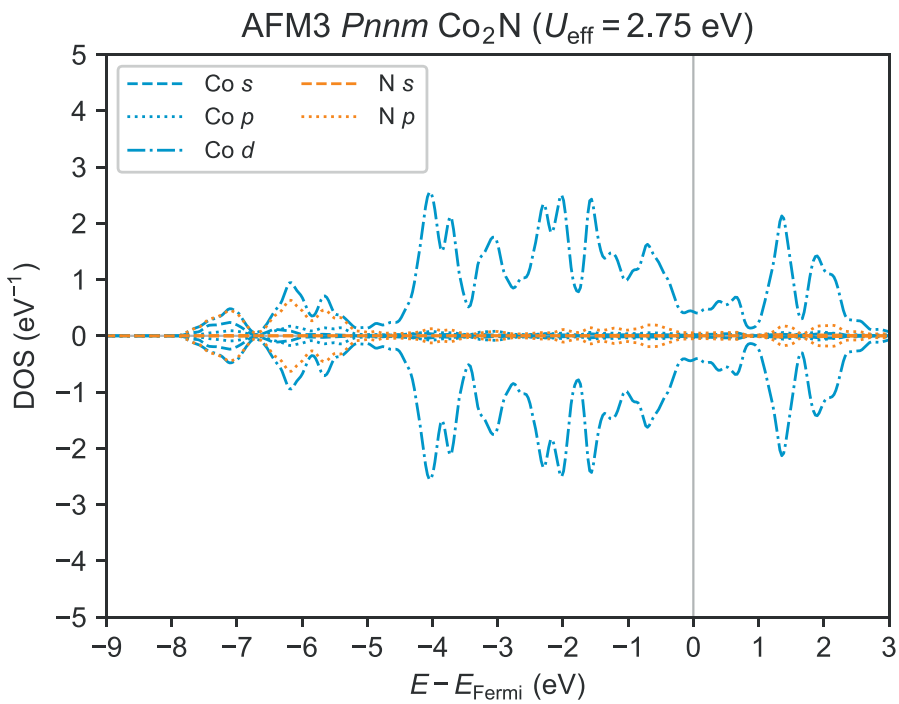

Fig. 9. Computed partial electronic DOS of AFM3 *Pnnm* Co_2N for $U_{eff} = 2.75$ eV. Positive and negative regions are for spin-up and spin-down components, respectively.

the magnetic moment of Co in the AFM3 state is about 2 μ_B, which is slightly higher than that of pure hcp Co, 1.715 μ_B [51].

Fig. 9 shows the computed partial electronic density of states (DOS) of AFM3 *Pnnm* Co_2N when $U_{eff} = 2.75$ eV. As expected, near the Fermi level, the Co *d* orbitals mainly contribute to the DOS. A nonzero DOS is found at the Fermi level, indicating its metallic nature.

5. Conclusions

In this paper, we have carefully revisited the phase stability of Co_2N based on both experiments and first-principles calculations. PXRD measurements clearly confirm that the stable Co_2N crystal structure adopts the space group *Pnnm* (isotype of η-Fe_2C and Co_2C) and not *Pbcn* (found for ζ-Fe_2N). The refined structural parameters of *Pnnm* Co_2N are $a = 4.6108(1)$ Å, $b = 4.3498(1)$ Å, $c = 2.85592(7)$ Å, $x = 0.3242(1)$, $y = 0.2643(1)$, with Co located at the 4*g* site of $(x,y,0)$. Based on first-principles calculations, we have revealed that with pure DFT calculations a wrong crystal structure and a wrong magnetic state are obtained for Co_2N and that it is therefore essential to consider strong on-site electron correlation to correctly obtain the experimentally confirmed stable AFM *Pnnm* Co_2N phase. In particular, an U_{eff} value of around 2.75 eV provides the correct ground state and a formation energy consistent with experiments. It has also been found that the energetic stability is sensitive to the detailed magnetic ordering. Our considered AFM3 state (cf. Fig. 2) provides a reasonable description of the correct phase stability of Co_2N and thus can be used in future studies of cobalt nitrides and oxynitrides at modest computational costs.

CRediT authorship contribution statement

Yuji Ikeda: Investigation, Formal analysis, Writing - original draft, Visualization. **Tanja S. Lehmann:** Investigation, Formal analysis. **Marc Widenmeyer:** Investigation, Formal analysis, Data curation, Writing - original draft. **Mauro Coduri:** Resources, Writing - review & editing. **Blazej Grabowski:** Writing - review & editing, Supervision, Project administration. **Rainer Niewa:** Conceptualization, Writing - review & editing, Supervision, Project administration.

Declaration of competing interest

The authors declare that they have no known competing financial interests or personal relationships that could have appeared to influence the work reported in this paper.

Acknowledgments

This work was supported by the European Research Council (ERC) under the EU's Horizon 2020 Research and Innovation Programme (Grant Agreement No. 639211). We also highly acknowledge the granted beam time and financial support by the European Synchrotron Radiation Facility, Grenoble, France.

References

[1] P. Höhn, R. Niewa, Nitrides of Non-Main Group Elements, Chap. 7, Wiley-VCH, Weinheim, 2017, pp. 251–359.
[2] M. Hasegawa, T. Yagi, Synthesis of Co_2N by a simple direct nitriding reaction between nitrogen and cobalt under 10 GPa and 1800 K using diamond anvil cell and YAG laser heating, Solid State Commun. 135 (5) (2005) 294–297, https://doi.org/10.1016/j.ssc.2005.05.009.
[3] G.T. Beilby, G.G. Henderson, The action of ammonia on metals at high temperatures, J. Chem. Soc. Trans. 79 (1901) 1245–1256, https://doi.org/10.1039/ct9017901245.
[4] X. Liu, H. Lu, M. He, K. Jin, G. Yang, H. Ni, K. Zhao, The preparation and antiferromagnetic properties of epitaxial rocksalt-type CoN films, J. Alloys Compd. 582 (2014) 75–78, https://doi.org/10.1016/j.jallcom.2013.08.001.
[5] K. Suzuki, T. Kaneko, H. Yoshida, H. Morita, H. Fujimori, Crystal structure and magnetic properties of the compound CoN, J. Alloys Compd. 224 (2) (1995) 232–236, https://doi.org/10.1016/0925-8388(95)01561-2.
[6] B. Das, M. Reddy, P. Malar, T. Osipowicz, G.S. Rao, B. Chowdari, Nanoflake CoN as a high capacity anode for Li-ion batteries, Solid State Ionics 180 (17–19)

(2009) 1061–1068, https://doi.org/10.1016/j.ssi.2009.05.007.
[7] K. Niwa, T. Terabe, D. Kato, S. Takayama, M. Kato, K. Soda, M. Hasegawa, Highly coordinated iron and cobalt nitrides synthesized at high pressures and high temperatures, Inorg. Chem. 56 (11) (2017) 6410–6418, https://doi.org/10.1021/acs.inorgchem.7b00516.
[8] R. Juza, W. Sachsze, Über das System Kobalt/Stickstoff, Z. Anorg. Allg. Chem. 253 (1–2) (1945) 95–108, https://doi.org/10.1002/zaac.19452530112.
[9] N. Terao, Transformations du cobalt sous l'influence de l'azote, Mem. Sci. Rev. Metall. 57 (1960) 96–100.
[10] P. Adamski, D. Moszyński, A. Komorowska, M. Nadziejko, A. Sarnecki, A. Albrecht, Ammonolysis of cobalt molybdenum oxides - in situ XRD study, Inorg. Chem. 57 (16) (2018) 9844–9850, https://doi.org/10.1021/acs.inorgchem.8b00685.
[11] D. Muller-Bouvet, J.-P. Pereira-Ramos, S. Bach, P. Willmann, A. Michalowicz, Effect of cobalt substitution on $Li_{3-2x}Co_xN$ local structure: a XAS investigation, Inorg. Chem. 53 (12) (2014) 6127–6131, https://doi.org/10.1021/ic500528f.
[12] S. Desmoulins-Krawiec, C. Aymonier, A. Loppinet-Serani, F. Weill, S. Gorsse, J. Etourneau, F. Cansell, Synthesis of nanostructured materials in supercritical ammonia: nitrides, metals and oxides, J. Mater. Chem. 14 (2) (2004) 228–232, https://doi.org/10.1039/b310806f.
[13] J.-S. Fang, L.-C. Yang, C.-S. Hsu, G.-S. Chen, Y.-W. Lin, G.-S. Chen, Phase transition behavior of reactive sputtering deposited Co–N thin films using transmission electron microscopy, J. Vac. Sci. Technol. A 22 (3) (2004) 698–704, https://doi.org/10.1116/1.1722656.
[14] M. Widenmeyer, L. Shlyk, N. Becker, R. Dronskowski, E. Meissner, R. Niewa, Synthesis of metastable Co_4N, Co_3N, Co_2N, and $CoO_{0.74}N_{0.24}$ from a single azide precursor and intermediates in $CoBr_2$ ammonolysis, Eur. J. Inorg. Chem. 2016 (29) (2016) 4792–4801, https://doi.org/10.1002/ejic.201600684.
[15] J. Clarke, K.H. Jack, The preparation and the crystal structures of Cobalt Nitride, Co_2N, of cobalt carbonitrides, $Co_2(C,N)$, and of Cobalt Carbide, Co_2C, Chem. Ind. 46 (46) (1951) 1004–1005.
[16] Y. Hirotsu, S. Nagakura, Crystal structure and morphology of the carbide precipitated from martensitic high carbon steel during the first stage of tempering, Acta Metall. 20 (4) (1972) 645–655, https://doi.org/10.1016/0001-6160(72)90020-x.
[17] D. Rechenbach, H. Jacobs, Structure determination of ζ-Fe_2N by neutron and synchrotron powder diffraction, J. Alloys Compd. 235 (1) (1996) 15–22, https://doi.org/10.1016/0925-8388(95)02097-7.
[18] L. Wang, T. Maxisch, G. Ceder, Oxidation energies of transition metal oxides within the GGA+U framework, Phys. Rev. B 73 (19) (2006) 195107, https://doi.org/10.1103/PhysRevB.73.195107.
[19] A. Herwadkar, W.R.L. Lambrecht, Electronic structure of CrN: a borderline Mott insulator, Phys. Rev. B 79 (3) (2009), https://doi.org/10.1103/PhysRevB.79.035125, 035125.
[20] B. Alling, T. Marten, I.A. Abrikosov, Effect of magnetic disorder and strong electron correlations on the thermodynamics of CrN, Phys. Rev. B 82 (18) (2010) 184430, https://doi.org/10.1103/PhysRevB.82.184430.
[21] L. Zhou, F. Körmann, D. Holec, M. Bartosik, B. Grabowski, J. Neugebauer, P.H. Mayrhofer, Structural stability and thermodynamics of CrN magnetic phases from *ab initio* calculations and experiment, Phys. Rev. B 90 (18) (2014) 184102, https://doi.org/10.1103/PhysRevB.90.184102.
[22] L.M. Corliss, N. Elliott, J.M. Hastings, Antiferromagnetic structure of CrN, Phys. Rev. 117 (4) (1960) 929–935, https://doi.org/10.1103/PhysRev.117.929.
[23] K. Momma, F. Izumi, *VESTA3* for three-dimensional visualization of crystal, volumetric and morphology data, J. Appl. Crystallogr. 44 (6) (2011) 1272–1276, https://doi.org/10.1107/S0021889811038970.
[24] M. Linhard, H. Flygare, Über komplexverbindungen. IV. Azido-pentamminkobalt(III)-komplexe, Z. Anorg. Allg. Chem. 262 (6) (1950) 328–343, https://doi.org/10.1002/zaac.19502620606.
[25] J. Rodríguez-Carvajal, Recent advances in magnetic structure determination by neutron powder diffraction, Physica B 192 (1–2) (1993) 55–69, https://doi.org/10.1016/0921-4526(93)90108-i.
[26] P.E. Blöchl, Projector augmented-wave method, Phys. Rev. B 50 (24) (1994) 17953–17979, https://doi.org/10.1103/PhysRevB.50.17953.
[27] J.P. Perdew, K. Burke, M. Ernzerhof, Generalized gradient approximation made simple, Phys. Rev. Lett. 77 (18) (1996) 3865–3868, https://doi.org/10.1103/PhysRevLett.77.3865.
[28] G. Kresse, J. Furthmüller, Efficient iterative schemes for *ab initio* total-energy calculations using a plane-wave basis set, Phys. Rev. B 54 (16) (1996) 11169–11186, https://doi.org/10.1103/PhysRevB.54.11169.
[29] G. Kresse, J. Furthmüller, Efficiency of *ab-initio* total energy calculations for metals and semiconductors using a plane-wave basis set, Comput. Mater. Sci. 6 (1) (1996) 15–50, https://doi.org/10.1016/0927-0256(96)00008-0.
[30] G. Kresse, D. Joubert, From ultrasoft pseudopotentials to the projector augmented-wave method, Phys. Rev. B 59 (3) (1999) 1758–1775, https://doi.org/10.1103/PhysRevB.59.1758.
[31] M. Methfessel, A.T. Paxton, High-precision sampling for Brillouin-zone integration in metals, Phys. Rev. B 40 (6) (1989) 3616–3621, https://doi.org/10.1103/PhysRevB.40.3616.
[32] S.L. Dudarev, G.A. Botton, S.Y. Savrasov, C.J. Humphreys, A.P. Sutton, Electron-energy-loss spectra and the structural stability of nickel oxide: an LSDA+U study, Phys. Rev. B 57 (3) (1998) 1505–1509, https://doi.org/10.1103/PhysRevB.57.1505.
[33] R.F.W. Bader, Atoms in Molecules: A Quantum Theory (International Series of Monographs on Chemistry), Clarendon Press, 1994, ISBN 9780198558651.
[34] M. Yu, D.R. Trinkle, Accurate and efficient algorithm for Bader charge integration, J. Chem. Phys. 134 (6) (2011), https://doi.org/10.1063/1.3553716, 064111.
[35] G. Henkelman, A. Arnaldsson, H. Jónsson, A fast and robust algorithm for Bader decomposition of charge density, Comput. Mater. Sci. 36 (3) (2006) 354–360, https://doi.org/10.1016/j.commatsci.2005.04.010.
[36] E. Sanville, S.D. Kenny, R. Smith, G. Henkelman, Improved grid-based algorithm for Bader charge allocation, J. Comput. Chem. 28 (5) (2007) 899–908, https://doi.org/10.1002/jcc.20575.
[37] W. Tang, E. Sanville, G. Henkelman, A grid-based Bader analysis algorithm without lattice bias, J. Phys. Condens. Matter 21 (8) (2009), https://doi.org/10.1088/0953-8984/21/8/084204, 084204.
[38] E.A. Owen, D.M. Jones, Effect of grain size on the crystal structure of cobalt, Proc. Phys. Soc. London Sect. B 67 (6) (1954) 456–466, https://doi.org/10.1088/0370-1301/67/6/302.
[39] T. Nishizawa, K. Ishida, The Co (cobalt) system, Bull. Alloy Phase Diagr. ISSN: 0197-0216 4 (4) (1983) 387–390, https://doi.org/10.1007/BF02868089.
[40] M.I. Aroyo (Ed.), International Tables for Crystallography, 6th ed., International Union of Crystallography, 2016 https://doi.org/10.1107/97809553602060000114.
[41] M. Widenmeyer, T.C. Hansen, A. Leineweber, A. Weidenkaff, R. Niewa, Nitrogen transfer between solid phases in the system Mn-N detected via *in situ* neutron diffraction, Z. Anorg. Allg. Chem. 643 (23) (2017) 1929–1938, https://doi.org/10.1002/zaac.201700304.
[42] M. Widenmeyer, T.C. Hansen, R. Niewa, Formation and decomposition of metastable α″-$Fe_{16}N_2$ from *in situ* powder neutron diffraction and thermal analysis, Z. Anorg. Allg. Chem. 639 (15) (2013) 2851–2859, https://doi.org/10.1002/zaac.201300379.
[43] M. Widenmeyer, T.C. Hansen, E. Meissner, R. Niewa, Formation and decomposition of iron nitrides observed by *in situ* powder neutron diffraction and thermal analysis, Z. Anorg. Allg. Chem. 640 (7) (2014) 1265–1274, https://doi.org/10.1002/zaac.201300676.
[44] H.A. Wriedt, N.A. Gokcen, R.H. Nafziger, The Fe-N (Iron-Nitrogen) system, Bull. Alloy Phase Diagr. 8 (4) (1987) 355–377, https://doi.org/10.1007/bf02869273.
[45] U. Schwarz, A. Wosylus, M. Wessel, R. Dronskowski, M. Hanfland, D. Rau, R. Niewa, High-pressure-high-temperature behavior of ζ-Fe_2N and phase transition to ε-$Fe_3N_{1.5}$, Eur. J. Inorg. Chem. 2009 (12) (2009) 1634–1639, https://doi.org/10.1002/ejic.200801222.
[46] B. Grabowski, T. Hickel, J. Neugebauer, *Ab initio* study of the thermodynamic properties of nonmagnetic elementary fcc metals: exchange-correlation-related error bars and chemical trends, Phys. Rev. B 76 (2) (2007), https://doi.org/10.1103/PhysRevB.76.024309, 024309.
[47] L. Pauling, The nature of the chemical bond. IV. The energy of single bonds and the relative electronegativity of atoms, J. Am. Chem. Soc. 54 (9) (1932) 3570–3582, https://doi.org/10.1021/ja01348a011.
[48] L.C. Allen, Electronegativity is the average one-electron energy of the valence-shell electrons in ground-state free atoms, J. Am. Chem. Soc. 111 (25) (1989) 9003–9014, https://doi.org/10.1021/ja00207a003.
[49] J.B. Mann, T.L. Meek, L.C. Allen, Configuration energies of the main group elements, J. Am. Chem. Soc. 122 (12) (2000) 2780–2783, https://doi.org/10.1021/ja992866e.
[50] J.B. Mann, T.L. Meek, E.T. Knight, J.F. Capitani, L.C. Allen, Configuration energies of the d-block elements, J. Am. Chem. Soc. 122 (21) (2000) 5132–5137, https://doi.org/10.1021/ja9928677.
[51] T. Kaneko, T. Kanomata, ε-Co, in: Y. Kawazoe, T. Kaneko, Y. Uwatoko (Eds.), Magnetic Properties of d-Elements, Alloys and Compounds under Pressure, Chap. 2.4, Springer, Berlin Heidelberg, 2014, pp. 16–17, https://doi.org/10.1007/978-3-642-41834-1_5.